Research Square

Preprints are preliminary reports that have not undergone peer review.
They should not be considered conclusive, used to inform clinical practice,
or referenced by the media as validated information.

CasPER reduces mutagenic repair during targeted transgene integration in human immune cells

Giovanni Pietrogrande

g.pietrogrande@uq.edu.au

The University of Queensland https://orcid.org/0000-0001-5107-2002

Tahmina Tabassum

The University of Queensland

Phoebe Dunbar

Peter MacCallum Cancer Centre

Alieh Fazeli

University of Freiburg

Pui Yeng Allie Lam

The University of Queensland https://orcid.org/0000-0003-4031-367X

Huiwen Zheng

The University of Queensland

Sandra Ammann

University of Freiburg

Tatjana Cornu

University of Freiburg

Bahaa Al-mhanawi

The University of Queensland

Melissa Elliot

The University of Queensland

Toni Cathomen

Medical Center - University of Freiburg https://orcid.org/0000-0002-7757-4630

Fernando Guimaraes

The University of Queensland https://orcid.org/0000-0002-2037-8946

Paul Beavis

Peter MacCallum Cancer Centre https://orcid.org/0000-0002-2116-013X

Ernst Wolvetang

The University of Queensland

Jake Bradford

Queensland University of Technology

Dimitri Perrin

Queensland University of Technology

Article

Keywords:

Posted Date: November 11th, 2026

DOI: https://doi.org/10.21203/rs.3.rs-11334597/v1

License: This work is licensed under a Creative Commons Attribution 4.0 International License.
Read Full License

Additional Declarations: There is a conflict of interest T.T., G.P. and E.W. are listed as inventors on patent PAT-02543-AU-01 covering CasPER. E.W. serves as a consultant for Valley Biosciences with financial interest and is co-founder and CSO of The Organoid Company B.V. F.S.F.G. is a Board Member of Cure Cancer Australia Foundation and a member of the Scientific Advisory Committee of ANZSA. Sanofi TSH, Microba Life Sciences and Cartherics sponsor research in the laboratory of F.S.F.G. P.A.B. declares research funding from Bristol-Myers-Squibb. P.K.D. declares research funding from Myeloid Therapeutics, Prescient Therapeutics, Bristol-Myers-Squibb and Juno Therapeutics. The remaining authors declare no competing interests.

Abstract

Efficient targeted integration is not necessarily safe: CRISPR–Cas9-induced DNA double-strand breaks can generate indels and chromosomal rearrangements even with highly specific gRNAs. Here, we developed CasPER (Cas9–PIAS4 for error reduction), a genome-editing platform that localises the SUMO E3 ligase PIAS4 to Cas9-induced breaks to modulate repair. Across multiple loci, cargo sizes, cell types and donos, CasPER maintained targeted transgene integration while reducing mutagenic indels and improving editing precision. The platform was compatible with plasmid-, mRNA- and RNP-based editor delivery and with linear DNA, circular DNA and AAV donor templates. In primary human NK cells, CasPER achieved knock-in comparable to Cas9 but generated fewer on-target indels. CAST-seq further showed that structural rearrangements can arise despite the absence of detectable off-target indels and that CasPER was associated with fewer distal rearrangement events. In primary human T cells, CasPER enabled targeted CAR insertion and generated functional CAR-T cells exhibiting tumour-cell killing, cytokine secretion and activation. Together, these findings distinguish cleavage specificity from repair fidelity and establish CasPER as a versatile platform for reducing genome-editing-associated mutagenesis while preserving therapeutically relevant cell function.

Introduction

Chimeric antigen receptor (CAR)-engineered immune cells have become an established therapeutic modality, particularly for haematological cancers (1). However, current manufacturing strategies remain complex, costly and rely largely on integrating viral vectors such as lentiviruses. Although these vectors enable efficient transgene delivery, they result in stochastic genomic integration, contributing to product heterogeneity and potential insertional mutagenesis (2–5). Targeted CAR integration at defined endogenous loci can instead provide more predictable transgene expression and a more uniform cell product, while simultaneously modifying endogenous regulators to enhance function. Such approaches can, for example, disrupt inhibitory signalling pathways in T cells and modulate cytotoxicity- or persistence-associated programmes in natural killer (NK) cells (6). However, CRISPR–Cas approaches carry their own genomic risks, including off-target cleavage, mutagenic repair outcomes and chromosomal abnormalities, particularly when large DNA cargos are introduced. Although mechanistically distinct from random lentiviral integration, these events can also disrupt genes or regulatory elements and remain an important barrier to clinical translation.

Pharmacological inhibition of non-homologous end joining using small molecules such as AZD7648 and M3814, which target the DNA-dependent protein kinase catalytic subunit (DNA-PKcs), can reduce indel formation and enhance homologous recombination during CRISPR-mediated genome editing, representing a promising strategy (7). However, despite increasing knock-in efficiency, these approaches globally perturb DNA-repair activity, potentially limiting their clinical translation. Indeed, DNA-PKcs inhibition has been associated with impaired cell viability and an increased frequency of chromosomal abnormalities (8). To avoid the cytotoxic and genotoxic consequences of globally perturbing DNA repair, several studies have fused components of the homologous recombination pathway directly to Cas9 or

its derivatives, thereby localising repair modulation to the Cas9 cleavage site (9). Although these engineered nucleases can improve precise integration, their efficacy remains strongly influenced by cellular context and target locus. Moreover, most designs recruit only a single DNA-repair component, which may be insufficient to coordinate the multiple steps required for efficient homologous recombination. These limitations underscore the need for more robust and broadly applicable strategies to control DNA-repair pathway choice.

We reasoned that tethering a catalytic enzyme capable of modifying multiple DNA-repair associated proteins directly to Cas9 could exert broader control over repair-pathway choice than recruiting a single repair factor. Based on this rationale, we developed CasPER (Cas9–PIAS4 for Error Reduction), a genome-editing platform in which CRISPR–Cas9 is fused to the SUMO E3 ligase PIAS4 and designed to locally modulate DNA repair through post-translational SUMOylation (Fig. 1a and Supplementary Fig. 1a). Previous studies have suggested that SUMOylation shapes chromatin accessibility, as well as DNA double-strand break signalling and repair (10–12). We therefore hypothesised that localising SUMO activity to Cas9-induced breaks could coordinate repair-factor assembly and chromatin responses in situ and bias repair towards homologous recombination. Here, we show that CasPER supports targeted transgene insertion across multiple clinically relevant loci, delivery formats, and primary immune-cell platforms like T and NK cells. Finally, CasPER reduced mutagenic chromosomal rearrangements in NK cells and enables efficient generation of functional CAR-T cells, supporting its use as a platform for more precise immune-cell engineering that preserves therapeutically relevant function.

Materials and methods

Structural prediction and molecular visualization

Protein structural predictions for CasPER were generated using AlphaFold2 (v2.0) and ColabFold. Structural rendering and molecular visualization were performed using PyMOL (v2.5, Schrödinger, LLC).

Cell line and primary cell culture

Human embryonic kidney (HEK293) cells were maintained in Dulbecco's Modified Eagle Medium/Nutrient Mixture F-12 (DMEM/F-12; Gibco) supplemented with 10% fetal bovine serum (FBS; Gibco) and 1% penicillin–streptomycin (100 U mL^{-1} penicillin, 100 µg mL^{-1} streptomycin; Gibco, cat. no. 15140122). K562 human lymphoblast cells were cultured in RPMI-1640 medium (Gibco, cat. no. 11875093) supplemented with 10% FBS and 1% penicillin–streptomycin. Human ovarian cancer cell line OVCAR-3 was obtained from American Type Culture Collection. Cells were confirmed as mycoplasma negative through polymerase chain reaction testing. OVCAR-3 cells were cultured in Roswell Park Memorial Institute (RPMI) 1640 medium supplemented with 10% heat-inactivated fetal bovine serum (FBS), 1 mM sodium pyruvate, 2 mM glutamine, 0.1 mM non-essential amino acids, 10 mM 4-(2-

hydroxyethyl)-1-piperazineethanesulfonic acid (HEPES), 100 U ml − 1 penicillin and 100 µg ml − 1 streptomycin (complete RPMI).

Primary NK cells were isolated from buffy coats provided by the Australian Red Cross as previously described (13). Primary NK cells were activated using irradiated K562 feeder cells. Seven days post-activation, NK cells were expanded in NK MACS medium (Miltenyi Biotec) supplemented with 5% heat-inactivated human AB serum, 500 IU mL^{-1} recombinant human IL-2 (Miltenyi Biotec, cat. no. 130-097-743), and 5 ng mL^{-1} human IL-15. Cells were maintained in 24-well plates at an initial seeding density of 5×10^5 cells mL^{-1}. Half-media exchanges were performed every 3 days, with complete media replacement conducted on day 7 via centrifugation at 300 × g for 5 min.

Primary human T cells were cultured and genome-edited as previously described (14). Human T cells were activated by isolating peripheral blood mononuclear cells from healthy buffy coats and culturing in complete RPMI containing human anti-CD3 (OKT3, Biolegend) (30 ng ml − 1) and hIL-2 (obtained from the National Institute of Health) (600 IU ml − 1) for 48 h. All cell lines were incubated at 37°C in a humidified atmosphere containing 5% CO_2.

Plasmid construction and gene editing reagents

All custom expression plasmids encoding CasPER and exogenous donor templates targeting the AAVS1, KLRC1, HBB, and B2M loci were designed using SnapGene (v6.2.1) and synthesized by VectorBuilder. The following pre-designed plasmid constructs were obtained from Addgene: empty gRNA backbone (#61424), Cas9/gRNA co-expression vector (#62988), 4.2 kb AAVS1-GFP donor vector (#22212), defective GFP (dGFP) reporter cassette (#113193), AAVS1 TALEN-L (#35431), and AAVS1 TALEN-R (#35432). Complete sequence maps are available via the Addgene repository.

To generate target-specific gRNA constructs, the empty gRNA backbone (Addgene #61424) was digested with BbsI, followed by ligation of annealed guide oligos using T4 DNA Ligase (Invitrogen). Ligation products were transformed into competent Escherichia coli cells (OneShot TOP10 or STBL3; Invitrogen) for clonal propagation, and accurate insertion was confirmed by Sanger sequencing.

To produce double-stranded linear homology donors (400, 600, or 800 bp homology arms), the GFP donor plasmid was engineered with flanked restriction sites, digested with appropriate restriction enzymes (New England Biolabs, NEB), and purified via agarose gel extraction.

In vitro-transcribed (IVT) CasPER mRNA and recombinant CasPER protein were manufactured by VectorBuilder. Recombinant Cas9 protein was obtained from VectorBuilder. Cas9 and GFP mRNAs were produced by Base Facility (University of Queensland) as described (15). Synthetic gRNAs were synthesized by Integrated DNA Technologies (IDT). Custom recombinant adeno-associated virus serotype 6 (AAV6) vectors containing AAVS1, KLRC1, and TRAC donor templates were produced by VectorBuilder.

Transfection and electroporation

For HEK293 transfections, cells were seeded into 24-well plates at 7×10^4 to 1×10^5 cells per well 24 h prior to transfection in antibiotic-free media. Plasmids were mixed at indicated molar ratios, diluted in Opti-MEM Reduced Serum Medium (Gibco), and co-transfected using Lipofectamine 2000 (Invitrogen) according to the manufacturer's protocol. Culture media was refreshed 48 h post-transfection. mRNA deliveries and plasmid co-deliveries were performed using Lipofectamine MessengerMAX (Invitrogen) following standard manufacturer procedures.

K562 cells were electroporated using the 4D-Nucleofector System (Lonza) equipped with the X Unit. Briefly, 2×10^5 cells were resuspended in 20 µL SF Cell Line Solution (V4XC-2021/2032) containing 150 ng of each plasmid and electroporated using program FF-120. Following pulse delivery, cells were incubated in the cuvette at room temperature for 10 min prior to transfer into 6-well plates containing pre-warmed media.

Primary NK cells were refreshed with media 24 h prior to nucleofection. Immediately prior to electroporation, 5 µg mRNA was complexed with 120 pmol synthetic gRNA in a total volume of 20 µL P3 Primary Cell Solution (Lonza, cat. no. V4XP-3032). NK cells were washed with PBS, pelleted at 250 × g for 5 min, and resuspended at 1×10^6 cells per cuvette. Electroporation was carried out using program DO-100. Cells were immediately recovered in pre-warmed NK medium. For homology-directed repair (HDR) experiments, AAV6 vectors carrying exogenous donor templates were added 5–10 min post-electroporation at a multiplicity of infection (MOI) of 5×10^4. Media was refreshed 24 h post-transduction.

T-cells were electroporated according to previously described parameters (14). To perform CRISPR/Cas9 editing, 37 pmol recombinant Cas9 (IDT) or CasPER and 270 pmol single guide RNA (sgRNA; Synthego) were combined and incubated at room temperature for 10 min to form Cas9/sgRNA ribonucleoprotein (RNP) complexes. Then, 1 × 106 T cells were resuspended in 20 µl X-VIVO 15 buffer (Lonza), combined with RNP and electroporated in 20-µl cuvettes using a 4D-Nucleofector X Unit (Lonza) with pulse code EO115. T cells were immediately washed out with prewarmed media to a concentration of 50 × 106 cells per millilitre and added to an appropriate culture plate containing a mixture of AAV6 at a multiplicity of infection (MOI) of 10,000 and 2 µM M3814 (MedChemExpress). T cells were incubated at 37°C for 4 h before AAV6 and M3814 were washed off and downstream protocols were performed. Homologous repair templates were manufactured and cloned by NotI digest into pAAV-MCS (Agilent Technologies) by Genscript, and the resulting plasmids were packaged into AAV6 vectors by PackGene Biotech.

Analysis of cytokine production

Supernatants from the in vitro co-culture assays were analysed for cytokine concentration using BD Cytometric Bead Array Flex sets for IFNγ (cat# 558269) and TNF (cat# 558273) (BD Biosciences). Data

were acquired using the FACSCanto II (BD Biosciences) and analysed using FlowJo and GraphPad Prism 10.

Chromium-51 release assay

Tumour cells were labelled with 51Cr by resuspending cell pellets in 50 µCi 51Cr per 1x106 cells and incubating at 37°C for 1 h. 1x104 51Cr-labelled tumour cells were then co-cultured with T cells at the indicated E:T ratios. As controls for background and total 51Cr levels, tumour cells were cultured either alone or with 5% Triton X-100 (Sigma-Aldrich). After a 16-h incubation, the 51Cr level in the supernatant was measured using the automatic gamma counter Wallac Wizard 1470 (PerkinElmer), and T cell killing was quantified using the following formula: [51Cr CPM (sample) − 51Cr CPM (background)]/[51Cr CPM (total) − 51Cr CPM (background)], where CPM stands for counts per minute.

Generation of the reporter HEK293T cell line

To establish a quantitative reporter for HDR, HEK293T cells were co-transfected with equimolar amounts of AAVS1-targeted TALEN-L and TALEN-R alongside the dGFP cassette (Addgene #113193) using Lipofectamine 2000. Stable integrants were selected with 200 µg mL^{-1} hygromycin for 3 weeks. To eliminate background fluorescence resulting from spontaneous intrachromosomal gene conversion, cells were subsequently subjected to puromycin selection for 1 week. The dGFP reporter contains multiple stop codons across an 18-bp non-frameshifting sequence and a truncated 5' GFP fragment serving as an internal repair template. Site-specific cleavage by Cas-endonucleases initiates homologous recombination (HR), restoring a functional GFP open reading frame (Fig. 1b).

Flow cytometry and cell sorting

For HR analysis, flow cytometry was performed 2–3 weeks post-nucleofection to ensure complete dilution and loss of unintegrated episomal donor vectors. GFP expression was quantified on a CytoFLEX (Beckman Coulter) or BD LSRFortessa cell analyzer, and data were processed using FlowJo software (v10; Tree Star). Forward scatter (FSC-A vs. FSC-H) and side scatter (SSC) parameters were applied to gate single, viable cells. Cell sorting (FACS) was performed at the QBI Flow Cytometry Facility and the Translational Research Institute (TRI) FlowCore (Brisbane, Australia).

To assess NK cell viability and immunophenotype, cells were stained with Zombie Violet Fixable Viability Kit (BioLegend) according to manufacturer instructions. Active primary NK populations were identified using the following antibody gating strategy: CD56 (Biolegend, #318332, 1:50), CD45(Biolegend, #304043, 1:400), CD3 (Biolegend, #317340, 1:200).

To assess T cell phenotype both in culture and post tumour stimulation, viable, single cells were stained with LIVE/DEAD™ Fixable Yellow Dead Cell Stain Kit (# L34959, Invitrogen, 1:800). Live cells were then gated on CD8 + T cells (BD, #612754, 1:1000). T cell phenotype was evaluated using CD69 (BD

Pharmigen, #557745, 1:200), CD45RA (BD Horizon, #562885, 1:1000), CD62L (BioLegend, #304814, 1:200), LAG3 (BioLegend, #369304, 1:200), TIM3 (BD Horizon, #565564, 1:600), FLAG (Biolegend, #637318, 1:400), TCRαβ (invitrogen, #12-9986-42, 1:100). Cells were incubated in FACS buffer (2% FBS, 2 mM EDTA in PBS) with fluorochrome-conjugated antibodies at 4°C for 30 min in the dark. Data was acquired on the FACSymphony A3 (BD Biosciences), and analysed using FlowJo software (v10; Tree Star). Acquisition was performed at the Research Flow Core, Peter MacCallum Cancer Centre.

Western Blot

HEK293 cells transfected with Cas9 or CasPER expression vectors were harvested 48 h post-transfection and lysed in RIPA buffer (Thermo Fisher Scientific) supplemented with 1× protease inhibitor cocktail. Cell lysates were sonicated using a single pulse (1 s at 40% intensity; VCX750, Sonics & Materials). Protein concentrations were quantified using the Pierce BCA Protein Assay Kit (Thermo Fisher Scientific, cat. no. 23225) against a bovine serum albumin (BSA) standard curve.

Total protein lysates (20 µg) were resolved on 4–20% precast polyacrylamide gels (Bio-Rad, cat. no. 17000436) and transferred onto PVDF membranes (Bio-Rad, cat. no. 1704156) using the Trans-Blot Turbo Transfer System (Bio-Rad). Membranes were blocked with 5% non-fat dry milk in Tris-buffered saline containing 0.1% Tween-20 (TBS-T) for 1 h at room temperature, followed by overnight incubation at 4°C with primary anti-Cas9 antibody (Cell Signaling Technology, cat. no. 14697S; 1:1,000). After three washes in TBS-T, membranes were incubated with horseradish peroxidase (HRP)-conjugated secondary antibodies for 1 h at room temperature. Chemiluminescent signals were developed using Clarity Western ECL Substrate (Bio-Rad, cat. no. 1705060) and imaged on a ChemiDoc MP Imaging System (Bio-Rad). Membranes were subsequently stripped using stripping buffer and re-probed with anti-β-actin antibody (Sigma-Aldrich, cat. no. A5441; 1:2,000) as a loading control.

PCR amplification and indel analysis

Target genomic regions were amplified using NEBNext High-Fidelity 2X PCR Master Mix (NEB, cat. no. M0541L) with target-specific primers (Table Y). Amplicons were purified using Qiagen or Monarch Gel Extraction / PCR Purification Kits according to the manufacturer's instructions.

For T7 Endonuclease I (T7EI) assays, 200 ng of purified PCR product was denatured and re-annealed in a thermal cycler, followed by enzymatic cleavage using T7 Endonuclease I (Alt-R Genome Editing Detection Kit; IDT, cat. no. 1075931) according to manufacturer instructions. Cleavage fragments were resolved on a 1% agarose gel.

For sequence decomposition analysis, purified PCR products were submitted for Sanger sequencing and analyzed using the TIDE web tool (16). Sequence traces were aligned against mock-transfected or wild-type controls using default parameters (maximum indel size of 20 bp; decomposition window set to maximal high-quality trace regions). For next-generation sequencing (NGS), target amplicons were subjected to paired-end 250 bp (PE250) sequencing on an Illumina platform. Library preparation and

high-throughput sequencing were conducted by GentleGen Sequencing (Guangzhou, China) and Novogene (Singapore). Raw sequencing reads were analyzed for editing efficiency using CRISPResso2 (v2.0)(17).

Whole genome sequencing

Genomic DNA from GFP⁺ HEK293 cells targeted at the AAVS1 locus with CasPER or Cas9 was extracted and submitted to GentleGen Biotech (Guangzhou, China) for 20× whole-genome sequencing (WGS). Candidate off-target loci were predicted using Cas-OFFinder (18) based on sequence homology with the target gRNA, and alignment datasets were screened using custom bioinformatic pipelines to evaluate potential off-target editing events.

Real-time quantitative PCR (RT-qPCR)

Total RNA was extracted from naïve and activated NK cells using the NucleoSpin RNA Kit (Macherey-Nagel / Scientificx) according to the manufacturer's protocol. Reverse transcription was performed with 500 ng of total RNA using the iScript cDNA Synthesis Kit (Bio-Rad). Quantitative PCR reactions were carried out using cDNA equivalent to 5 ng of input RNA with PowerUp SYBR Green Master Mix (Applied Biosystems) on a CFX Opus Real-Time PCR Detection System (Bio-Rad). Relative expression levels were normalized to hypoxanthine phosphoribosyltransferase 1 (HPRT) as an internal reference gene using primers listed on Supplementary Table 1.

CAST-Seq

Genomic DNA was extracted using the Qiagen DNeasy Kit according to the manufacturer's protocol. CAST-Seq analyses were performed according to (19) and leveragingan improved algorithm to classify chromosomal rearrangements (20). In brief, 500 ng of genomic DNA were used as input material for each technical replicate. Libraries were prepared using the NEBNext® Ultra™ II FS DNA Library Prep Kit for Illumina (NEB E7805L). Enzymatic fragmentation of the genomic DNA was aimed at an average length of 500–800 bp. CAST-Seq libraries were sequenced on a NovaSeq using 2x150 bp paired-end sequencing (GENEWIZ, Azenta Life Sciences). For each sample, 2 technical replicates library preparations were run and analysed. Only sites that were present in both technical replicates and significant in at both replicates are shown in the circos plots. For sites under investigation, the spacer sequence of the gRNA was aligned to the most covered regions for each site (± 400 bp). Sites were labelled as OMT if any of the two p-values reached the cutoff of 0.005. Two decoy primers and bait primers on the telomeric side were used.

Precision Score

The precision score was calculated for each sample as the ratio of precise editing frequency to on-target indel frequency. Precise editing was quantified by flow cytometry as GFP restoration or targeted GFP knock-in, whereas on-target indels were measured by TIDE or targeted next-generation sequencing in the corresponding cell population. This metric was adapted from a previously described approach for comparing outcomes between genome-editing platforms (21).

Statistical analysis

Statistical analyses were performed using GraphPad Prism (version X). Data are presented as the mean ± s.e.m. unless otherwise indicated. Individual data points represent biological or technical replicates, as specified in the figure legends. Statistical significance was assessed using *t*-tests or analysis of variance with the appropriate multiple-comparisons test, as indicated in each figure legend. Exact *P* values are reported for prespecified comparisons, with $P \geq 0.05$ considered not significant.

Results

Improved HR mediated precise gene correction using CasPER

A HEK293T defective GFP (dGFP) reporter cell line was generated by TALEN-mediated integration of a constitutively expressed dGFP cassette (Addgene plasmid #113193) at the *AAVS1* locus (22). HDR-mediated correction of the defective sequence restores GFP expression (Fig. 1b and Supplementary Fig. 1b). GFP-positive and GFP-negative populations were isolated by FACS and analysed by Sanger sequencing. Accurate repair of the 18-bp region was observed in GFP-positive cells, whereas GFP-negative cells showed a high frequency of indels, confirming that the system reliably reports successful HDR events (Fig. 1c). We next compared the performance of Cas9 and Cas9 fused to PIAS4 (CasPER) (Supplementary Fig. 1d). Transfection efficiency, transgene expression, and plasmid retention were comparable across conditions (Supplementary Fig. 1e). Maximal GFP correction was observed 5 days post-transfection, showing a slower kinetics than previously reported (Supplementary Fig. 1f) (23). Exploratory assessment of on-target indel formation after two weeks by T7E1 assay showed a reduction in CasPER-treated cells relative to Cas9 (Supplementary Fig. 1g).

To directly compare Cas9- and CasPER-mediated repair outcomes, vector-positive (BFP^+) cells and cells exhibiting restored GFP expression (GFP^+) were enriched by FACS 48 h after transfection (Fig. 1c). Cas9 produced modestly higher GFP-restoration frequencies than CasPER (~ 15% versus ~ 10%; Fig. 1d). However, this increase was accompanied by substantially greater indel formation, as Sanger sequencing of the dGFP locus followed by TIDE analysis (16) revealed indel frequencies of ~ 70% with Cas9 compared with ~ 10% with CasPER (Fig. 1e and Supplementary Fig. 1h). A similar trend was also observed in the GFP negative sorted population (Supplementary Fig. 1i). We then confirmed the results with targeted next-generation sequencing (NGS) of the dGFP locus analysed with CRISPResso2.0 (17). Consistent with previous results, CasPER showed significantly reduced indel frequencies (< 20%) compared to Cas9 (> 40%) (Fig. 1f). Finally, to quantify editing fidelity, we used the precision score (21), calculated within each sample as the ratio of precise repair frequency, measured by GFP restoration or knock-in, to mutagenic indel frequency, determined by TIDE or targeted NGS. This metric was used throughout subsequent experiments to identify conditions favouring precise over mutagenic repair. Using this metric, CasPER exhibited an approximately 3-fold higher precision score compared to Cas9 (Fig. 1g).

Cell type and gene target impact CasPER performance in large gene insertion

Although the dGFP reporter provided initial evidence that CasPER improves editing precision relative to Cas9, this system relies on intrachromosomal homologous recombination and may not reflect editing outcomes when donor DNA is supplied exogenously. We therefore evaluated CasPER for large-transgene knock-in, an application in which integration efficiency is strongly influenced by cell type, target locus, chromatin context and donor configuration (9). Because CasPER activity was expected to depend partly on the endogenous DNA-repair environment, we profiled PIAS4 alongside the HR regulators RAD51 and BRCA1 and the NHEJ-associated factor RIF1 across candidate cell types. Both BRCA1 and RIF1 have been reported to undergo PIAS4-dependent SUMOylation (11, 24). HEK293 and K562 cells were selected as experimentally tractable adherent and haematopoietic models, respectively, because they expressed these factors at levels broadly comparable to those observed in human peripheral blood mononuclear cells (PBMCs) and Natural Killer (NK) cells, providing a relevant benchmark for subsequent experiments (Supplementary Fig. 2a). We then compared large-transgene knock-in efficiencies between Cas9 and CasPER across these distinct cellular contexts (Fig. 2a).

To optimise donor suitability, we first assessed the effect of homology-arm length on targeted GFP integration at the *AAVS1* safe-harbour locus in HEK293 cells. Among linear double-stranded DNA donors carrying 400-, 600- or 800-bp homology arms, the 800-bp design yielded the highest integration efficiency with both Cas9 and CasPER (Fig. 2b-c). We next compared donor topology using the optimised 800-bp homology arms and found that linear donors supported higher integration efficiencies than circular plasmid donors, consistent with previous reports (25)(Fig. 2d). We preliminary investigated off-target activity by whole-genome sequencing at a mean coverage of 20× on FACS-sorted GFP-positive cells (Supplementary Fig. 2b). Many SNVs were detected across the genome, consistent with the substantial genomic instability and aneuploidy characteristic of HEK293 cells, which limited the suitability of this approach for evaluating off-target editing. Nevertheless, Cas-OFFinder identified approximately 13,000 potential off-target sites for the *AAVS1* gRNA (27), fewer than 0.2% of which contained detectable SNVs, with a trend towards fewer affected sites in CasPER-edited cells than in Cas9-edited cells (Supplementary Fig. 2c).

We next assessed the safety of CasPER editing at four clinically relevant loci: the safe harbour *AAVS1*, *B2M*, *HBB* and *KLRC1*. The *B2M* locus is a promising candidate site for CAR insertion in T cells (26), whereas mutations in *HBB* are responsible for several blood disorders, including sickle cell anaemia and β-thalassaemia (27). *KLRC1* was selected as a clinically relevant locus of interest for NK-cell engineering because of its established role in regulating antitumour activity (27). Prioritising specificity over predicted editing efficiency, we screened published and novel candidate gRNAs using two complementary tools: COSMID (28) and CHOPCHOP (29) prediction algorithms and integrated their outputs to identify the guide with the highest predicted specificity. Notably, the selected *KLRC1* gRNA had previously demonstrated high editing efficiency in NK cells (30), but its genomic safety profile had

not been investigated. This provided an opportunity to determine whether an efficient guide also possessed the specificity required for future therapeutic development and whether CasPER could further improve repair fidelity. The selected gRNAs were initially screened by editing K562 cells with the optimized 800-bp ds-linear donor template and we compared the performance of CasPER and Cas9. FACS analysis showed that GFP knock-in efficiency varied across the targeted loci, and CasPER efficiency was comparable or higher than what achieved with Cas9 (Fig. 2e). Among the loci examined, *KLRC1* (Supplementary Fig. 2d) showed the greatest relative improvement with CasPER and was therefore selected for further investigation. We investigated the indel rate at this locus (Supplementary Fig. 2e) and found that CasPER showed a 2.3-fold higher precision score than Cas9 (Fig. 2f). Before extending this approach to a more clinically relevant setting in primary cells, we confirmed its compatibility with a non-plasmid delivery format in K562 cells. Delivery of mRNA encoding each editor together with a synthetic gRNA and an AAV6 donor did not alter the relative editing performance of CasPER and Cas9 compared with the plasmid-based system used in the preceding experiments (Supplementary Fig. 2f).

CasPER improves repair fidelity during high-specificity KLRC1 editing

Having observed greater editing precision with CasPER at the *KLRC1* locus, we next evaluated its capacity to support large-transgene integration in primary human NK cells. To assess feasibility and genomic safety in a clinically relevant configuration, Cas9 or CasPER were delivered as mRNA and with a donor template by AAV6, consistent with other ex vivo gene-editing protocols (31, 32). Previous reports showed distinct DNA-repair gene-expression profiles in resting and activated NK cells: pro-NHEJ genes were robustly expressed in both states, whereas pro-HR gene expression increased following activation (31). We therefore examined DNA-repair regulators by qPCR in resting and cytokine-activated primary NK cells from two healthy donors (Supplementary Fig. 3a). Consistent with the previous report (30), expression of the pro-NHEJ regulator, RIF1 remained high and did not differ significantly between states, whereas activated NK cells exhibited higher expression of pro-HR regulators (12-fold for BRCA1 and 31-fold for RAD51). Based on these findings, all subsequent editing experiments were performed in cytokine-activated NK cells. Primary NK cells were isolated from healthy donors, expanded (Fig. 3a) and confirmed to maintain a $CD45^{+}CD56^{+}$ phenotype before editing (Supplementary Fig. 3b)(33). Cells were then nucleofected with Cas9 or CasPER mRNA using an optimised protocol (Supplementary Fig. 3c-d) (29), transduced with the AAV6 donor and could be further expanded (Supplementary Fig. 3e). The mRNA nucleofection protocol was independently validated using GFP-encoding mRNA, yielding approximately 95% GFP-positive cells with minimal inter-donor variability (Supplementary Fig. 3f-g). For targeted integration, the AAV6 donor contained a 1.3-kb GFP expression cassette driven by the constitutive SFFV promoter and flanked by 800-bp homology arms corresponding to the targeted *KLRC1* region. SFFV was selected because it drives higher transgene expression in human NK cells than other commonly used strong promoters, including CAG and CMV (34). Using this workflow, Cas9 and CasPER achieved substantial and comparable levels of GFP knock-in, which remained stable from day 7 to day 14 (Fig. 3b and Supplementary Fig. 3h). Although editing efficiencies and indel frequencies varied among

donors (Supplementary Fig. 3i–k), analysis across independent donors and experiments confirmed that CasPER generated significantly fewer indels at the targeted *KLRC1* locus (Fig. 3c) and achieved a significantly higher editing precision score than Cas9 (Fig. 3d).

We next assessed sequence-level off-target editing and performed NGS at four candidate sites nominated for the *KLRC1* gRNA using two independent prediction tools (Supplementary Table 1). No insertions or deletions were detected within ± 10 bp of the predicted cleavage site at any locus in either Cas9- or CasPER-edited cells. Within a narrower ± 1-bp window, raw sequencing reads contained only sporadic substitutions below the predefined variant-calling threshold (Supplementary Fig. 4a). Thus, none of the candidate sites exhibited a detectable cut-site-associated indel signal suggesting a high sequence specificity of the *KLRC1* gRNA under the tested conditions.

To extend the analysis beyond *in silico*–predicted sites and assess structural genomic outcomes using a prediction-independent approach, we performed after four days CAST-seq (19, 20) on paired Cas9- and CasPER-edited samples from donor D241, which exhibited the highest on-target indel frequency among the three donors edited. Both editors generated a similar incidence of rearrangements at the targeted *KLRC1* locus across the technical replicates with independent library preparations (Fig. 3e and Supplementary Fig. 4c). However, CasPER-edited cells exhibited fewer rearrangements involving distal genomic loci compared to Cas9 (Fig. 3f and Supplementary Table 1). Specifically, among OMTs reproducibly detected across both technical replicates, 21 loci were unique to Cas9-edited cells, one was unique to CasPER-edited cells and five were shared between conditions (Fig. 3g and Supplementary Fig. 4d). Circos analysis further showed that rearrangements involved fewer chromosomes in CasPER-edited cells than in Cas9-edited cells (5 vs 15; Fig. 3h), and relative CAST-seq enrichment at reproducibly detected distal loci was lower in CasPER-edited samples (Supplementary Fig. 4e). To assess local indel formation at CAST-seq-nominated rearrangement partners, we performed rhAmpSeq at all loci shared between Cas9- and CasPER-edited samples, together with the six highest-ranking editor-specific candidates for each nuclease. Because fewer than six CasPER-specific loci passed the reproducibility threshold, the CasPER panel was supplemented with the highest-ranking candidates detected in only one technical replicate (Supplementary Table 1). Robust indel formation was confirmed at the *KLRC1* on-target site, whereas no cut-site-associated indel enrichment was detected at any nominated distal locus in either condition (Fig. 3i). Thus, any local indel activity at the CAST-seq-nominated loci, if present, was below the ~ 0.1% detection threshold of rhAmpSeq under the tested conditions. Importantly, although CAST-seq identified distal rearrangements with both editors, the rearrangement rate was markedly lower in CasPER-edited samples, with fewer affected loci and lower signals than in Cas9-edited samples.

RNP-delivered CasPER enables the generation of functional TRAC-targeted CAR-T cells

Having demonstrated CasPER-mediated editing following mRNA delivery in primary NK cells, we next evaluated whether the platform could be delivered extended to another format (RNP, ribonucleoprotein) and another cell type of interest (primary T cells, Fig. 4a). Because primary T cells are typically activated

before genome editing to promote expansion and efficient genetic modification, we analysed published transcriptomic data from resting and activated T cells (35). *PIAS4* expression remained comparatively low throughout the 72-h activation period (Fig. 4b), whereas NHEJ-associated genes were generally more highly expressed than HR-associated genes (Fig. 4c and Supplementary Fig. 5a). This repair profile provided a relevant context in which to test whether localised PIAS4 activity could improve editing outcomes. Cas9 or CasPER RNPs were then used to generate *TRAC*-targeted LeY CAR-T cells. To mirror the high-specificity targeting context established in NK cells, we selected a *TRAC* gRNA with no detectable off-target activity in previous genome-wide analysis (36, 37). We then assessed whether CasPER could support CAR integration at this clinically relevant locus and generate CAR-T cells with antigen-dependent effector function.

Primary T cells from healthy donors were edited using Cas9 or CasPER RNPs together with an AAV6 donor encoding the LeY CAR for targeted insertion at the *TRAC* locus (14). Flow cytometry showed no significant difference in overall editing efficiency between Cas9 and CasPER (Supplementary Fig. 5b), although the distribution of editing outcomes differed between the two editors (Fig. 4d). CasPER generated significantly fewer $TCR^{-}FLAG^{+}$ cells but significantly more $TCR^{+}FLAG^{+}$ cells, consistent with a shift towards CAR integration with retained TCR expression (Fig. 4e). CasPER-treated cultures also contained a significantly higher proportion of $TCR^{+}FLAG^{-}$ cells, consistent with reduced TRAC knockout in the absence of CAR integration. Under the same sampling conditions used for NK-cell CAST-seq, targeted sequencing showed an indel frequency of approximately 50% following Cas9 editing, whereas it remained below 10% following CasPER editing (Fig. 4f). Although consistent with reduced mutagenic repair, the low indel frequency in the CasPER condition precluded a reliable matched CAST-seq comparison, which requires sufficient on-target activity in both experimental arms to remain within the assay's detection range.

We next assessed the functionality of CasPER-generated CAR-T cells from three independent donors to determine the reproducibility of the approach. These cells exhibited CAR-dependent killing of LeY-positive tumour cells (Fig. 4g and Supplementary Fig. 5c) and responded to tumour-cell exposure by increasing secretion of the pro-inflammatory cytokines IFNγ and TNFα (Fig. 4h-i and Supplementary Fig. 5d). Tumour-cell exposure also significantly increased the percentage of $CD69^{+}$ cells (Fig. 4j and Supplementary Fig. 5e). Altogether, these phenotypic changes were consistent with antigen-induced activation, induction of inhibitory-receptor expression and differentiation away from a naïve-like state towards a more differentiated effector phenotype. Overall, these results establish the compatibility of CasPER with RNP delivery and primary T-cell engineering, enabling the generation of functional TRAC-targeted LeY CAR-T cells using a clinically relevant workflow and a highly specific gRNA.

Discussion

Here, we show that CasPER improves targeted-editing precision across multiple genomic loci, cell types and delivery formats. Experiments in HEK293 and K562 cells established that CasPER supports gene correction and large-transgene knock-in across different donor configurations while reducing mutagenic

indel formation. We then extended the platform to primary NK and T cells, delivering CasPER as mRNA and RNP, respectively, and demonstrated improved repair precision at the clinically relevant *KLRC1* and *TRAC* loci while preserving targeted integration and cellular function. To our knowledge, CasPER represents the first fusion of Cas9 to a SUMO E3 ligase. Unlike approaches that recruit an individual repair factor, CasPER was designed to localise PIAS4-dependent SUMOylation at Cas9-induced breaks and thereby modulate multiple components of the repair response. By profiling PIAS4 together with key HR- and NHEJ-associated factors across cell types and activation states, we explicitly considered the endogenous repair environment when evaluating CasPER rather than treating it as a context-independent editor. Targeted integration avoids the stochastic transgene insertion associated with conventional integrating viral vectors. However, CRISPR-induced double-strand breaks introduce distinct risks, including indels, large deletions, inversions and translocations (38). High-fidelity nucleases and highly specific gRNAs reduce unintended cleavage but cannot prevent repair-associated alterations arising from the intended break. Indeed, CAST-seq analysis has shown that HiFi Cas9 can reduce off-target-mediated translocations without eliminating homology-mediated or on-target rearrangements (19). Editing safety therefore depends on both where cleavage occurs and how the resulting break is repaired.

We first evaluated CasPER in primary human NK cells using mRNA delivery of the editor and AAV6 delivery of the donor template, extending previous NK-cell knock-in studies based on RNP delivery (31, 39). CasPER produced GFP knock-in at *KLRC1* at levels comparable to Cas9 while significantly reducing on-target indel formation and increasing editing precision. Safety analyses at *KLRC1* provided strong evidence for the sequence-level specificity of the selected gRNA. Targeted deep sequencing detected no cut-site-associated indels at four candidate sites nominated across three prediction algorithms. CAST-seq extended this analysis beyond *in silico* predictions by identifying distal loci involved in structural rearrangements, none of which showed local indel enrichment upon rhAmpSeq validation. Thus, off-target cleavage was not detectable by either prediction-guided NGS or prediction-independent CAST-seq nomination followed by targeted deep sequencing. Nevertheless, CAST-seq detected structural rearrangements involving the targeted *KLRC1* locus with both editors. In the donor analysed, on-target rearrangement profiles were similar, whereas CasPER was associated with fewer rearrangements involving distal genomic regions. The absence of local indels at these distal loci indicates that they should be considered rearrangement patterns rather than confirmed sites of off-target cleavage. These findings confirm that unwanted structural genomic outcomes can arise even when a highly specific gRNA is used and may escape detection by conventional amplicon sequencing. CasPER did not eliminate this risk but reduced indel formation and distal rearrangement-associated outcomes, providing an additional layer of risk reduction following cleavage.

We next extended CasPER to primary T cells using RNP delivery and an AAV6 donor carrying a LeY CAR targeted to *TRAC*. The selected gRNA had previously undergone genome-wide off-target analysis, providing a validated high-specificity targeting context (36). Although CasPER generated fewer $TCR^{-}FLAG^{+}$ cells and a greater proportion of $TCR^{+}FLAG^{+}$ and phenotypically unedited cells, it substantially reduced on-target indel formation. Importantly, CasPER-generated CAR-T cells from three independent donors retained CAR-dependent tumour-cell killing, cytokine secretion and activation-

associated phenotypic responses. CasPER is therefore compatible with both mRNA- and RNP-based delivery and can generate functionally active engineered NK and T cells. A matched CAST-seq comparison could not be performed in T cells because the low CasPER-induced indel frequency fell below the activity range required for reliable analysis; accordingly, these experiments establish functional applicability rather than independent evidence of structural genomic safety in T cells.

More broadly, our findings raise the hypothesis that endogenous repair-factor profiles could guide the selection of repair-modulating Cas9 fusions for different therapeutic cell types. CasPER may be particularly advantageous in cells with relatively low PIAS4 expression but preserved downstream HR capacity, where tethering PIAS4 to Cas9 could locally supplement a limiting activity without globally perturbing DNA repair. The same principle could extend to cell types limited by other repair regulators, such as RAD51 or BRCA1, through the development of editors that recruit the corresponding activity. Another alternative is provided by DSB-independent platforms such as PASTE, which exhibit favourable safety and low off target indels profiles (40); however, their potential to generate rare structural abnormalities remains incompletely defined. Here, we show that CasPER can be combined with highly specific gRNAs exhibiting minimal detectable sequence-level off-target activity while reducing distal rearrangement-associated outcomes, providing an approach to dampen genomic risk in DSB-based editing.

Together, our findings support a layered approach to editing safety in which nuclease and gRNA specificity limit unintended cleavage, while CasPER reduces mutagenic repair following cleavage. By retaining targeted integration and therapeutically relevant cellular function while decreasing indels and distal rearrangement-associated outcomes, CasPER provides a strategy with the potential to improve the genomic safety of engineered immune cells.

Ethics declarations

All experiments conducted in this study used human-derived materials in compliance with ethical guidelines and were approved by the Human Research Ethics Committee (HREC) at the University of Queensland (approval number: 2023/HE000027). Buffy coats from healthy donors less than 35 years old were obtained from the Red Cross with informed consent, as approved by the Red Cross and the Peter MacCallum Cancer Centre (PMCC) Human Research and Ethics Committee under HREC#01/14.

Declarations

Competing interests

T.T., G.P. and E.W. are listed as inventors on patent PAT-02543-AU-01 covering CasPER. E.W. serves as a consultant for Valley Biosciences with financial interest and is co-founder and CSO of The Organoid Company B.V. F.S.F.G. is a Board Member of Cure Cancer Australia Foundation and a member of the Scientific Advisory Committee of ANZSA. Sanofi TSH, Microba Life Sciences and Cartherics sponsor

research in the laboratory of F.S.F.G. P.A.B. declares research funding from Bristol-Myers-Squibb. P.K.D. declares research funding from Myeloid Therapeutics, Prescient Therapeutics, Bristol-Myers-Squibb and Juno Therapeutics. The remaining authors declare no competing interests.

Authors and Affiliations

Australian Institute for Bioengineering and Nanotechnology, The University of Queensland, St Lucia, QLD 4072, Australia

Tahmina Tabassum, Giovanni Pietrogrande, Ernst Wolvetang, Huiwen Zheng, Bahaa Al-mhanawi

Department of Biochemistry and Biotechnology, North South University, Dhaka 1229, Bangladesh

Tahmina Tabassum

Frazer Institute, Faculty of Health, Medicine and Behavioural Sciences, The University of Queensland, Woolloongabba, QLD 4102, Australia

Fernando Souza-Fonseca-Guimaraes, Allie Lam, Melissa Elliott

Institute for Transfusion Medicine and Gene Therapy, Medical Center - University of Freiburg, Freiburg, Germany

Sandra Ammann, Alieh Fazeli, Toni Cathomen

Center for Chronic Immunodeficiency, Medical Center – University of Freiburg, Freiburg, Germany

Tatjana Cornu, Sandra Ammann, Alieh Fazeli, Toni Cathomen

Faculty of Medicine, University of Freiburg, Freiburg, Germany

Sandra Ammann, Toni Cathomen

Cancer Immunology Program, Peter MacCallum Cancer Centre, Melbourne, Victoria, Australia.

Paul A. Beavis and Phoebe A. Dunbar

Sir Peter MacCallum Department of Oncology, The University of Melbourne, Parkville, Victoria, Australia.

Paul A. Beavis and Phoebe A. Dunbar

School of Computer Science, Queensland University of Technology (QUT), Brisbane, QLD, Australia

Jake Bradford and Dimitri Perrin

Author Contributions

Conceptualisation: T.T., G.P., E.W.; Methodology: T.T., G.P.; NK cells: T.T., F.S.F.G., A.L., M.E.; T cells: P.D., P.B.; Computational analysis: T.T.,H.Z.,G.P.; Western Blot: B.A., T.T.; CASTseq: A.F., S.A., T.C.,T.T.,T.C., Structural Prediction: M.H. All authors have reviewed and approved the final manuscript.

Acknowledgement

G.P. and T.T. were supported by the Australian Research Council grant ARC DP210103401. T.T. was supported by the Australian Government Research Training Program (RTP) Scholarship provided by the University of Queensland. P.A.B. is a CRI Lloyd J. Old STAR (CRI5578) and was supported by an NHMRC Investigator grant (L1; APP2042524); T.C., A.F., S.A. were supported by CAR Factory (funded by German Cancer Aid). F.S.F.G. is funded by a grant (#2019485) awarded through the Medical Research Future Fund (MRFF) in a co-funded partnership with the QLD Children's Hospital Foundation, Microba Life Sciences, Miltenyi Biotec, the Richie's Rainbow Foundation, the Translational Research Institute (TRI), and UQ; a grant (#NCRIXXIV000019) awarded through MRFF NCRI in a co-funded partnership with Cooper Rice-Brading Foundation (CRBF), Richie's Rainbow Foundation, TRI, Australia Red Cross Lifeblood, QLD Government, UQ and UNSW; a grant from the National Breast Cancer Foundation (#2023/IIRS0063); a grant (#IG250200299) awarded through the Australian Economic Accelerator (AEA); a grant (#2026-0039) awarded through the Ovarian Cancer Research Foundation; and funding from the CRBF, The Tie Dye Project, The Kids Cancer Project, Bricks & Smiles, Tour de Cure, and the PA Research Foundation. The content is solely the responsibility of the authors and does not necessarily represent the official views of the organisations and funding agencies. Illustrations were created using BioRender.com and modified.

References

1. Al-khreisat MJ, Abdulsahib WK, Jasim IK, Malathi H, Nayak PP, Anand DA, et al. Next-generation CAR-T and CAR-NK cell therapies in hematologic malignancies: engineering for persistence, specificity, and safety. *Discover Oncology.* 2026;17(1):524.
2. Bot A, Scharenberg A, Friedman K, Guey L, Hofmeister R, Andorko JI, et al. In vivo chimeric antigen receptor (CAR)-T cell therapy. *Nat Rev Drug Discov.* 2026;25(2):116–37.
3. Berg P, Ruppert-Seipp G, Müller S, Maurer GD, Hartmann J, Holtick U, et al. CAR T-cell-associated secondary malignancies challenge current pharmacovigilance concepts. *EMBO Mol Med.* 2025;17(2):211–8.
4. Willyard C. Do cutting-edge CAR-T-cell therapies cause cancer? What the data say. *Nature.* 2024;629(8010):22–4.
5. Elsallab M, Ellithi M, Lunning MA, D'Angelo C, Ma J, Perales M-A, et al. Second primary malignancies after commercial CAR T-cell therapy: analysis of the FDA Adverse Events Reporting System. *Blood.*

2024;143(20):2099–105.

6. Zhang J, Hu Y, Yang J, Li W, Zhang M, Wang Q, et al. Non-viral, specifically targeted CAR-T cells achieve high safety and efficacy in B-NHL. *Nature.* 2022;609(7926):369–74.
7. Selvaraj S, Feist WN, Viel S, Vaidyanathan S, Dudek AM, Gastou M, et al. High-efficiency transgene integration by homology-directed repair in human primary cells using DNA-PKcs inhibition. *Nature Biotechnology.* 2024;42(5):731–44.
8. Cullot G, Aird EJ, Schlapansky MF, Yeh CD, van de Venn L, Vykhlyantseva I, et al. Genome editing with the HDR-enhancing DNA-PKcs inhibitor AZD7648 causes large-scale genomic alterations. *Nature Biotechnology.* 2025;43(11):1778–82.
9. Tabassum T, Pietrogrande G, Healy M, and Wolvetang EJ. CRISPR-Cas9 Direct Fusions for Improved Genome Editing via Enhanced Homologous Recombination. *International Journal of Molecular Sciences.* 2023;24(19):14701.
10. Altmannova V, Eckert-Boulet N, Arneric M, Kolesar P, Chaloupkova R, Damborsky J, et al. Rad52 SUMOylation affects the efficiency of the DNA repair. *Nucleic Acids Res.* 2010;38(14):4708–21.
11. Galanty Y, Belotserkovskaya R, Coates J, Polo S, Miller KM, and Jackson SP. Mammalian SUMO E3-ligases PIAS1 and PIAS4 promote responses to DNA double-strand breaks. *Nature.* 2009;462(7275):935–9.
12. Ryu H-Y, and Hochstrasser M. Histone sumoylation and chromatin dynamics. *Nucleic Acids Research*. 2021;49(11):6043–52.
13. Wong JKM, McCulloch TR, Alim L, Omer N, Mehdi AM, Tuong ZK, et al. TGF-β signalling limits effector function capacity of NK cell anti-tumour immunity in human bladder cancer. *eBioMedicine.* 2024;104.
14. Chen AXY, Yap KM, Kim JS, Sek K, Huang Y-K, Dunbar PA, et al. Rewiring endogenous genes in CAR T cells for tumour-restricted payload delivery. *Nature.* 2025;644(8075):241–51.
15. Leighton LJ, Chaudhary N, Tompkins HT, Kulkarni A, Carrodus NL, Budzinska MA, et al. The design, manufacture and LNP formulation of mRNA for research use. *Nature Protocols.* 2025;20(12):3552–81.
16. Brinkman EK, and van Steensel B. Rapid Quantitative Evaluation of CRISPR Genome Editing by TIDE and TIDER. *Methods Mol Biol.* 2019;1961:29–44.
17. Pinello L, Canver MC, Hoban MD, Orkin SH, Kohn DB, Bauer DE, and Yuan G-C. Analyzing CRISPR genome-editing experiments with CRISPResso. *Nature Biotechnology.* 2016;34(7):695–7.
18. Bae S, Park J, and Kim J-S. Cas-OFFinder: a fast and versatile algorithm that searches for potential off-target sites of Cas9 RNA-guided endonucleases. *Bioinformatics.* 2014;30(10):1473–5.
19. Turchiano G, Andrieux G, Klermund J, Blattner G, Pennucci V, el Gaz M, et al. Quantitative evaluation of chromosomal rearrangements in gene-edited human stem cells by CAST-Seq. *Cell Stem Cell.* 2021;28(6):1136-47.e5.

20. Rhiel M, Geiger K, Andrieux G, Rositzka J, Boerries M, Cathomen T, and Cornu TI. T-CAST: An optimized CAST-Seq pipeline for TALEN confirms superior safety and efficacy of obligate-heterodimeric scaffolds. *Frontiers in Genome Editing.* 2023;Volume 5–2023.
21. Carusillo A, Haider S, Schäfer R, Rhiel M, Türk D, Chmielewski Kay O, et al. A novel Cas9 fusion protein promotes targeted genome editing with reduced mutational burden in primary human cells. *Nucleic Acids Research*. 2023;51(9):4660–73.
22. Sanjana NE, Cong L, Zhou Y, Cunniff MM, Feng G, and Zhang F. A transcription activator-like effector toolbox for genome engineering. *Nature Protocols.* 2012;7(1):171–92.
23. Brinkman EK, Chen T, de Haas M, Holland HA, Akhtar W, and van Steensel B. Kinetics and Fidelity of the Repair of Cas9-Induced Double-Strand DNA Breaks. *Molecular Cell.* 2018;70(5):801 – 13.e6.
24. Kumar R, and Cheok CF. Dynamics of RIF1 SUMOylation is regulated by PIAS4 in the maintenance of Genomic Stability. *Scientific Reports.* 2017;7(1):17367.
25. Yao X, Zhang M, Wang X, Ying W, Hu X, Dai P, et al. Tild-CRISPR Allows for Efficient and Precise Gene Knockin in Mouse and Human Cells. *Dev Cell.* 2018;45(4):526 – 36.e5.
26. Liu X, Zhang Y, Cheng C, Cheng AW, Zhang X, Li N, et al. CRISPR-Cas9-mediated multiplex gene editing in CAR-T cells. *Cell Research.* 2017;27(1):154–7.
27. Almasoudi HH. Therapeutic promise of CRISPR-Cas9 gene editing in sickle cell disease and β-thalassemia: A current review. *Curr Res Transl Med.* 2025;73(3):103513.
28. Cradick TJ, Qiu P, Lee CM, Fine EJ, and Bao G. COSMID: A Web-based Tool for Identifying and Validating CRISPR/Cas Off-target Sites. *Molecular Therapy Nucleic Acids.* 2014;3.
29. Labun K, Montague TG, Gagnon JA, Thyme SB, and Valen E. CHOPCHOP v2: a web tool for the next generation of CRISPR genome engineering. *Nucleic Acids Research.* 2016;44(W1):W272-W6.
30. Bexte T, Albinger N, Al Ajami A, Wendel P, Buchinger L, Gessner A, et al. CRISPR/Cas9 editing of NKG2A improves the efficacy of primary CD33-directed chimeric antigen receptor natural killer cells. *Nature Communications.* 2024;15(1):8439.
31. Naeimi Kararoudi M, Likhite S, Elmas E, Yamamoto K, Schwartz M, Sorathia K, et al. Optimization and validation of CAR transduction into human primary NK cells using CRISPR and AAV. *Cell Reports Methods.* 2022;2(6).
32. Li JH, Zhou A, Lee CD, Shah SN, Ji JH, Senthilkumar V, et al. MEF2C regulates NK cell effector functions through control of lipid metabolism. *Nature Immunology.* 2024;25(5):778–89.
33. Caligiuri MA. Human natural killer cells. *Blood.* 2008;112(3):461–9.
34. Silvestre RN, Eitler J, Azevedo JTC, Malmegrim KCR, Swiech K, Covas DT, et al. PROMOTER CHOICE: THE IDEAL PROMOTER TO DRIVE CHIMERIC ANTIGEN RECEPTOR (CAR) EXPRESSION IN NK CELLS. *Hematology, Transfusion and Cell Therapy*. 2021;43:S268-S9.
35. Rade M, Böhlen S, Neuhaus V, Löffler D, Blumert C, Merz M, et al. A time-resolved meta-analysis of consensus gene expression profiles during human T-cell activation. *Genome Biology.* 2023;24(1):287.

36. Kaeuferle T, Stief TA, Canzar S, Kutlu NN, Willier S, Stenger D, et al. Genome-wide off-target analyses of CRISPR/Cas9-mediated T-cell receptor engineering in primary human T cells. *Clinical & Translational Immunology.* 2022;11(1):e1372.
37. Kath J, Du W, Pruene A, Braun T, Thommandru B, Turk R, et al. Pharmacological interventions enhance virus-free generation of TRAC-replaced CAR T cells. *Mol Ther Methods Clin Dev.* 2022;25:311–30.
38. Ruis BL, Bielinsky AK, and Hendrickson EA. Gene editing and CRISPR-dependent homology-mediated end joining. *Experimental & Molecular Medicine.* 2025;57(7):1409–18.
39. Shankar K, Zingler-Hoslet I, Tabima DM, Zima S, Shi L, Gimse K, et al. Virus-free CRISPR knockin of a chimeric antigen receptor into < em>KLRC1 generates potent GD2-specific natural killer cells. *Molecular Therapy.* 2025;33(3):1014–30.
40. Yarnall MTN, Ioannidi EI, Schmitt-Ulms C, Krajeski RN, Lim J, Villiger L, et al. Drag-and-drop genome insertion of large sequences without double-strand DNA cleavage using CRISPR-directed integrases. *Nat Biotechnol.* 2023;41(4):500–12.

Figures

Figure 1

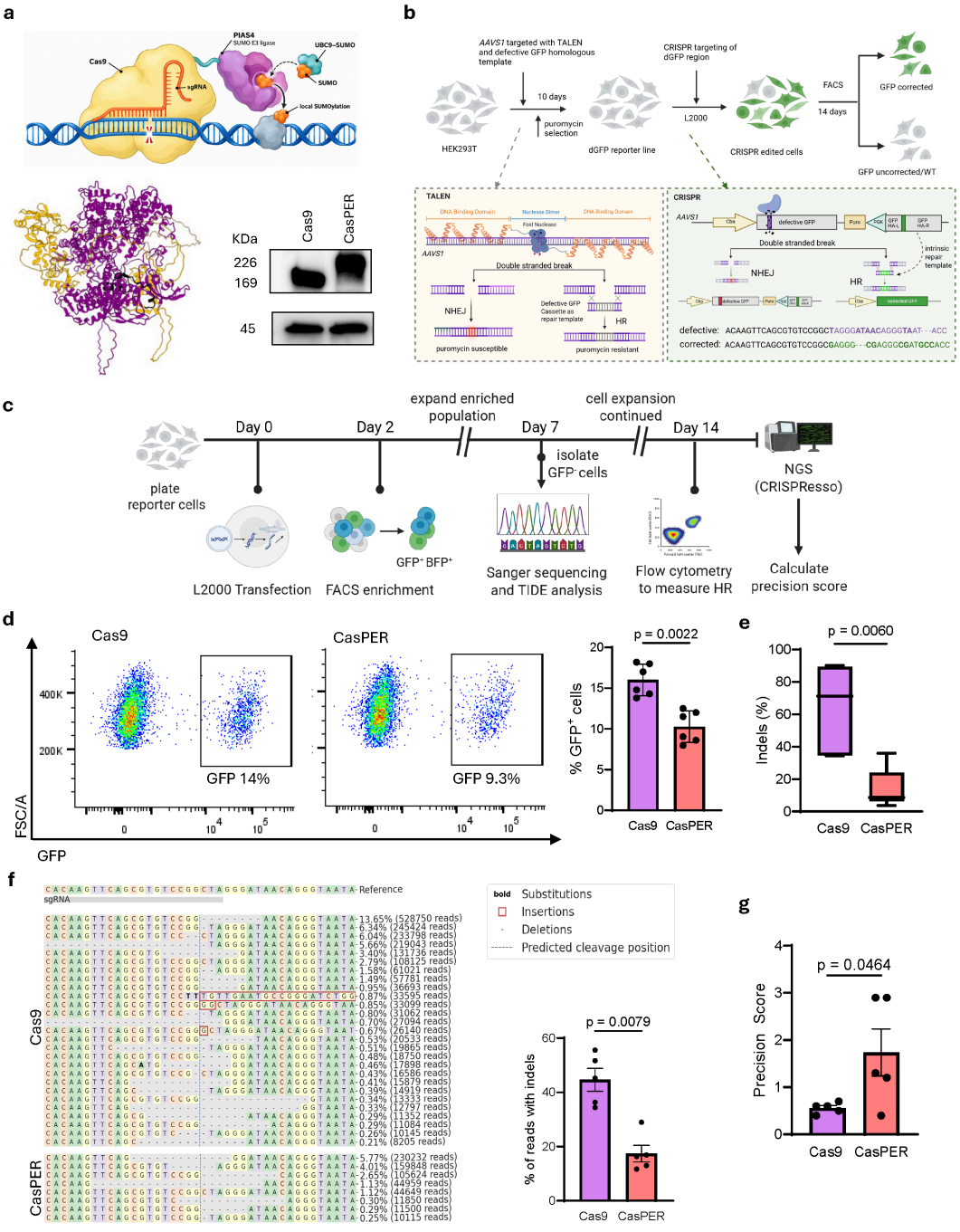


Figure 1

CasPER maintains precise gene correction while reducing mutagenic repair.

a Schematic of the proposed CasPER mechanism, in which fusion of the SUMO E3 ligase PIAS4 to Cas9 localises SUMOylation activity to Cas9-induced DNA double-strand breaks. The domain organisation and top-ranked AlphaFold2 model show Cas9 (purple) and PIAS4 (yellow) separated by an intervening

3×FLAG tag (black). Immunoblot analysis confirms Cas9 and CasPER expression in HEK293 cells 48 h after transfection; β-actin was used as a loading control. **b**Schematic of reporter cell-line generation and the dGFP correction assay. The dGFP cassette was integrated at the *AAVS1* locus and restored through homologous recombination with an internal repair template. **c**Experimental workflow and timeline for the head-to-head comparison of Cas9 and CasPER, including cell enrichment, flow cytometry, Sanger sequencing with TIDE analysis and targeted next-generation sequencing. **d** Representative flow-cytometry plots and quantification of HR-mediated GFP restoration 14 days after editing with Cas9 or CasPER. **e** On-target indel frequencies at the dGFP target site determined by TIDE analysis. **f** Representative CRISPResso2 classification of targeted sequencing reads into precise correction and quantification of mutagenic outcomes. **g** Editing precision score, calculated for each sample as the ratio of HR-mediated correction to on-target indel formation, showing an approximately threefold higher score with CasPER than with Cas9. Data are presented as the mean ± SEM; n = 6 samples across two independent experiments in **d** and n = 5 samples in **e–g**. Statistical significance was determined using t Mann-Whitney test in **d**, **e** and **g**. Exact P values are shown in the figure.

Figure 2

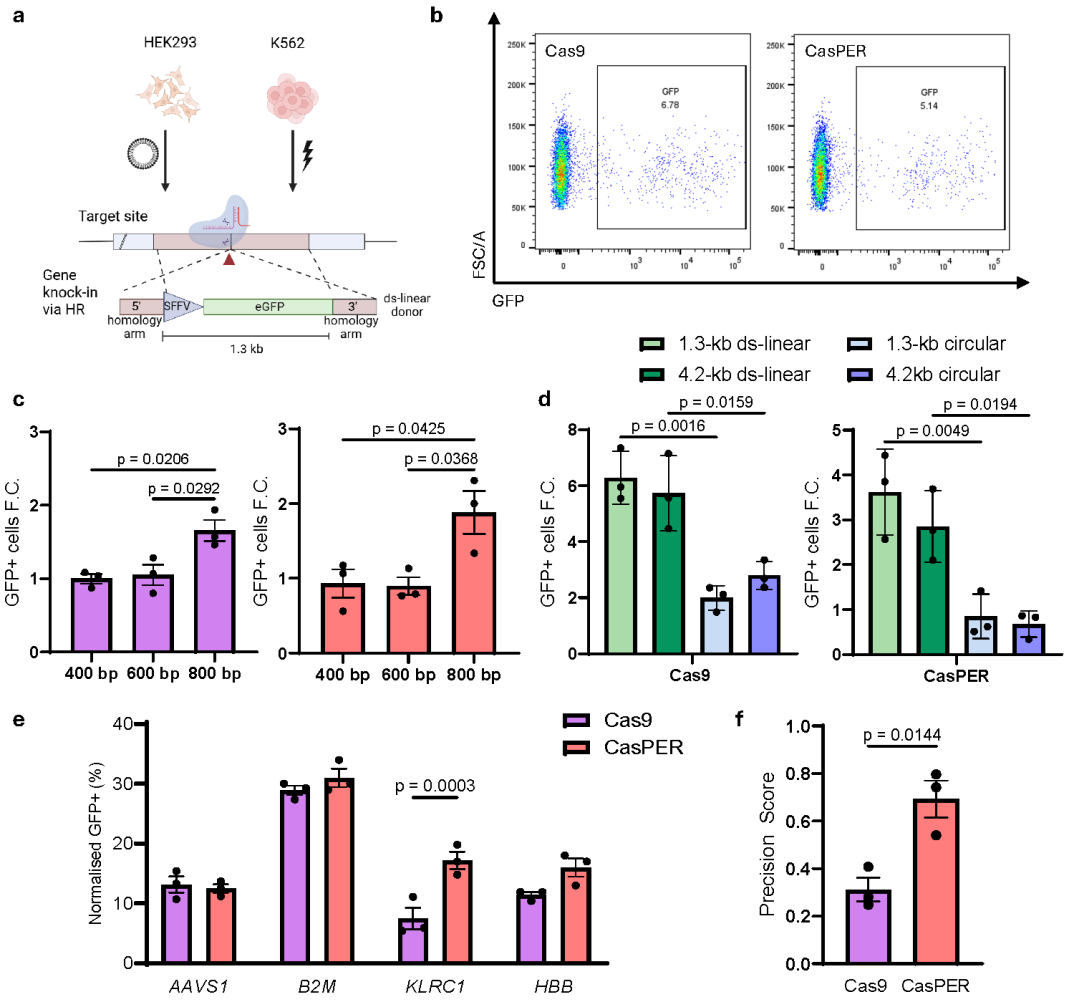


Figure 2

CasPER supports context-dependent large-transgene insertion across loci and delivery formats.

a Schematic of the experimental workflows used for GFP knock-in in HEK293 and K562 cells, with plasmid-based editing components delivered by lipofection and electroporation, respectively. For *AAVS1* targeting, the donor contained a 1.3-kb GFP expression cassette driven by the spleen focus-forming virus

(SFFV) promoter and flanked by 800-bp homology arms. **b**Representative flow-cytometry plots of GFP knock-in at the *AAVS1* locus in HEK293 cells using a linear double-stranded DNA (dsDNA) donor. **c**Quantification of GFP knock-in following Cas9 or CasPER editing using linear dsDNA donors with 400-, 600- or 800-bp homology arms. **d** Comparison of GFP knock-in at the *AAVS1* locus using linear dsDNA or circular plasmid donors containing 1.3- or 4.2-kb cargoes flanked by 800-bp homology arms. **e**GFP knock-in at the *AAVS1*, *B2M*, *KLRC1* and *HBB* loci in K562 cells using linear dsDNA donors with 800-bp homology arms. GFP-positive cells were quantified by flow cytometry after 3 weeks of expansion. **f**Editing precision at the *KLRC1* locus, calculated for each sample as the ratio of GFP knock-in efficiency to on-target indel frequency. CasPER increased the mean precision score 2.33-fold relative to Cas9. Data are presented as the mean ± SEM from $n = 3$ biological replicates unless otherwise indicated. Statistical significance was assessed using two-way ANOVA followed by Tukey's multiple-comparisons test in **c–e** and a two-tailed *t*-test in **f**. Exact *P*values are shown in the figure.

Figure 3

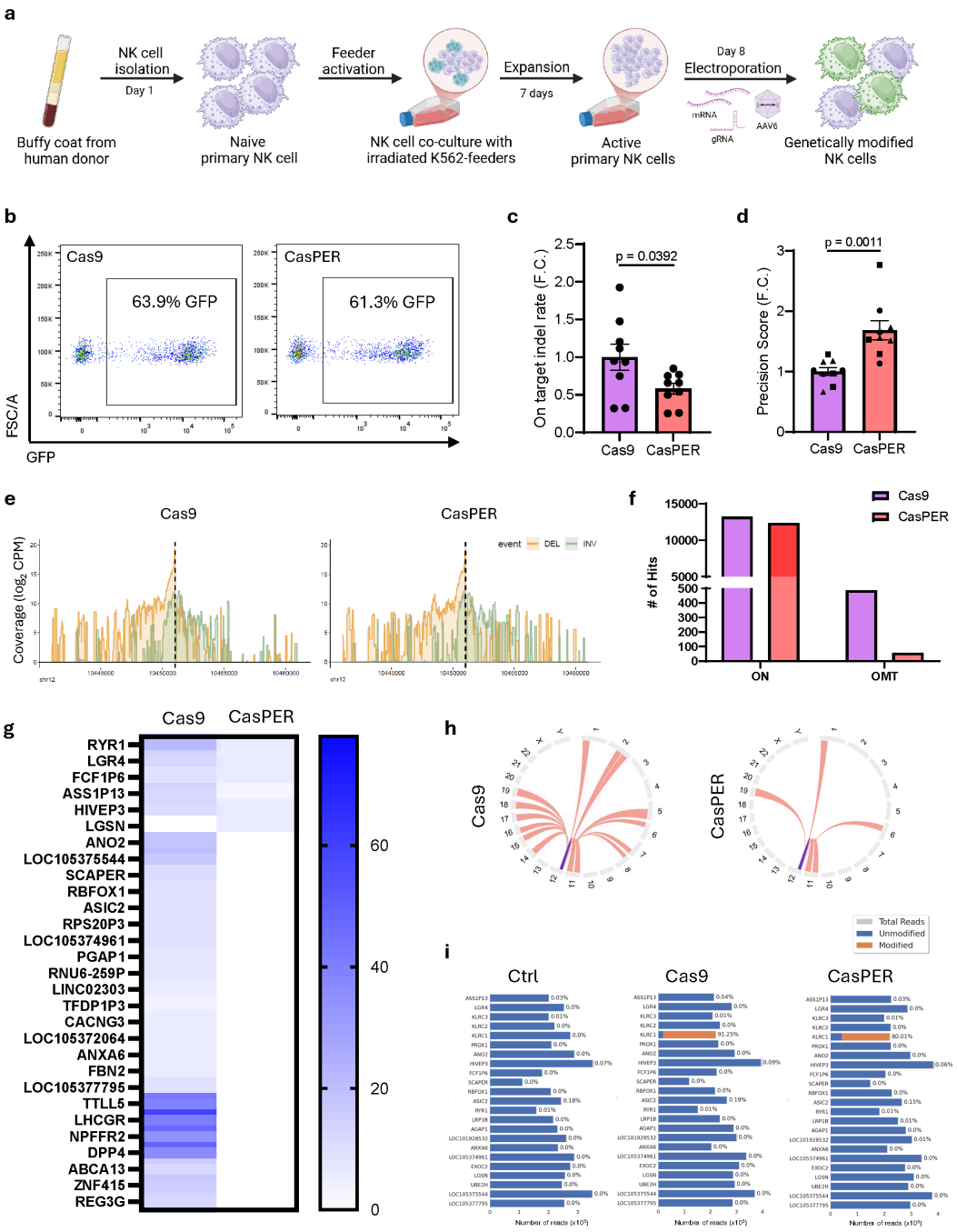


Figure 3

CasPER maintains knock-in efficiency while reducing mutagenic repair in primary human NK cells.

a Schematic overview of primary human NK-cell isolation, expansion, genetic modification and analysis. **b** Representative flow cytometry plots of GFP knock-in in primary NK cells edited (D241) with Cas9 or CasPER and analysed 5 days after editing. **c** On-target indel frequencies at the KLRC1 locus, determined

by TIDE analysis. **d** Precision score across all donors. Data in **c** and **d**were obtained from three independent donors with three technical replicates per donor (n = 9). **e** Frequency of deletion (orange) and inversion (green) events at the targeted KLRC1 locus in Cas9- and CasPER-edited cells. **f**Total number of NHEJ-associated events identified by CAST-seq at the on-target locus (ON) and off-target-mediated translocation sites (OMT) in Cas9- and CasPER-edited cells. **g** Heatmap showing the absolute number of deduplicated CAST-seq hits supporting rearrangement junctions at each distal genomic locus in Cas9- and CasPER-edited samples. **h** Circos plot of Cas9 and CasPER samples showing distribution of chromosomal rearrangements confirmed in both technical replicates. **i** Results of rhAmp seq NGS in control not transduced, and Cas9 or CasPER transduced NK cells. Data are presented as the mean ± SEM, Mann-Whitney test.

Figure 4

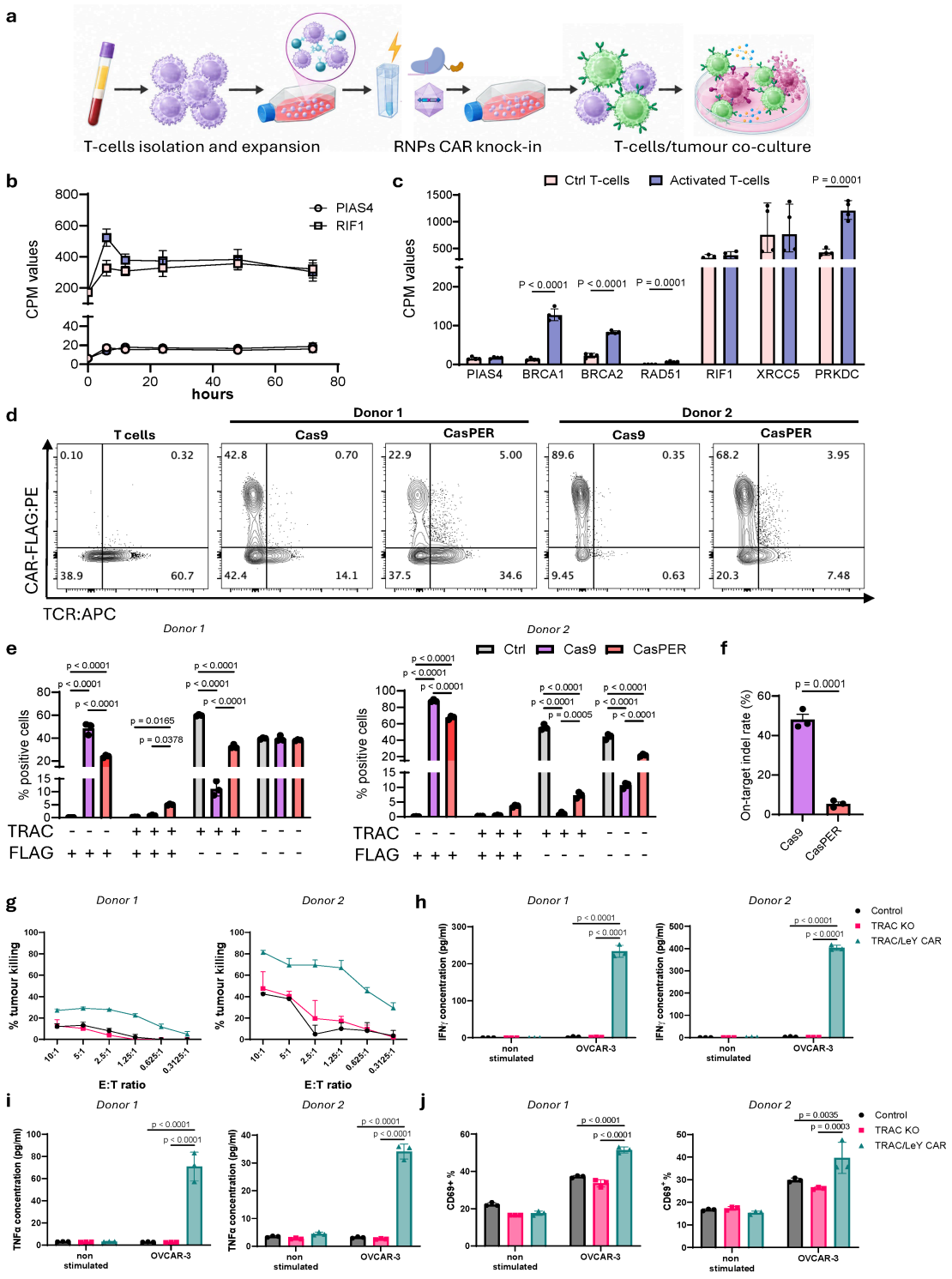


Figure 4

CasPER generates functionally active TRAC-targeted CAR-T cells

a Schematic overview of primary human T-cell isolation, expansion, genetic modification and functional analysis. **b.** Bulk RNA-sequencing analysis of gene expression in human T cells before activation and over the subsequent 72 h, reported as counts per million (CPM). **c.** Expression of *PIAS4*, HR-associated

genes (*BRCA1*, *BRCA2* and *RAD51*) and NHEJ-associated genes (*RIF1*, *XRCC5* and *PRKDC*) at 24 h after activation compared with donor-matched unstimulated controls. Data were obtained from four independent donors. **d** Representative flow cytometry plots of primary human T cells following targeted LeY CAR insertion at the TRAC locus. CAR–FLAG expression and loss of TCR expression were used to quantify targeted CAR integration and TRAC disruption, respectively. **e**Quantification of targeted CAR integration and TRAC disruption in primary T cells from two independent donors (n = 3 technical replicates per donor). **f** On-target indel frequencies at the TRAC locus after four days from transduction, determined by TIDE analysis (n = 3). **g**Specific lysis of ^51Cr-labelled LeY-positive OVCAR-3 tumour cells following co-culture with unedited control T cells, TRAC-KO T cells or TRAC-targeted LeY CAR-T cells at the indicated effector-to-target (E) ratios, as determined using a ^51Cr-release assay (n = 3 technical replicates). **h, i** Concentrations of IFN-γ (**h**) and TNF-α (**i**) in culture supernatants from unedited control, TRAC KO and TRAC-targeted LeY CAR-T cells cultured alone (unstimulated) or co-cultured with OVCAR-3 tumour cells, as quantified by Cytometric Bead Array. **j**Percentage of $CD69^+$ T cells following culture alone or stimulation with OVCAR-3 tumour cells, as determined by flow cytometry. Data are presented as the mean ± SEM, n=3 technical replicates per donor, Mann-Whitney or Tukey's multiple comparison test.

Supplementary Files

This is a list of supplementary files associated with this preprint. Click to download.

- T.TabassumetalSupplementaryFigures.pdf
- T.TabassumetalSupplementaryTable1.xlsx
- T.TabassumetalSupplementary.pdf